Ab initio intraband contributions to the optical properties of metals

Marco Cazzaniga,* Lucia Caramella,† Nicola Manini, and Giovanni Onida
Università degli Studi di Milano, Physics Department, and European Theoretical Spectroscopy Facility (ETSF), via Celoria 16, 20133 Milano, Italy

(Received 28 May 2010; revised manuscript received 17 June 2010; published 7 July 2010)

We introduce a method, based on the linearization of the band dispersion, to include intraband contributions in *ab initio* calculations of the optical spectra of metals. We illustrate its application to cubic iron and hexagonal magnesium, by analyzing the contributions of interband and intraband transitions to the dielectric function and the optical conductivity. These calculations demonstrate a way to compute the conductivity anisotropy of noncubic metals without the need to resort to phenomenological parametrizations. In particular, we introduce a method to recover the correct asymptotic trend of the response functions in the $\omega \to 0$ limit and hence compare directly with the experimental static conductivity.

DOI: 10.1103/PhysRevB.82.035104 PACS number(s): 71.15.Mb, 71.20.−b, 78.20.−e, 75.50.Bb

I. INTRODUCTION

Optical properties of solids belong to the class of material properties which can be successfully predicted by today's state of the art theoretical and numerical tools. In the case of semiconductor and insulating materials, recent developments allow one to go beyond the simple independent quasiparticle approximation[1] hence including electron-electron and electron-hole interaction effects,[2,3] and substantially improving the agreement with experimental data.

In the latest years, efficient methods have been introduced in order to make calculations for nonmetallic systems faster and more efficient.[4–7] Metallic systems, on the other hand, are generally not so badly described in the independent quasiparticle approximation because of the much more efficient screening experienced by quasiparticles in metals. Even in rather highly correlated systems such as the transition metals, the simple random phase approximation (RPA) was shown to work fairly well.[8–11] However, the calculation of optical spectra of gapless systems must face another difficulty, which does not appear in semiconductors and insulators: the necessity to include intraband transitions. The currently standard approach to intraband contributions relies on the determination of a single plasma frequency, leading to the addition of a phenomenological Drude contribution to the one produced by the interband transitions.[8] This simple "plasma model" approach has two obvious shortcomings: (i) it is intrinsically isotropic, which is fine for cubic crystals but is certainly inappropriate for noncubic metals and (ii) it ignores the crystal local field (CLF). Metallic screening is indeed expected to mitigate the effect of CLF but, for consistency sake, the fully *ab initio* inclusion of CLF is desirable anyway. In Ref. 10 an approximate treatment was proposed; more recently a rather intricate method based on time-dependent current-density-functional theory has also been applied to metals.[12]

In the present work we propose an approach for accurate and systematic inclusion of intraband contributions to the optical response on the same footing as interband ones, thus avoiding the discussed limitations. This method has the advantage of involving a simple and straightforward physical formalism, and is not especially computationally expensive. To include interband transitions explicitly, one should, in principle, evaluate the long-wavelength response by considering intraband transitions down to a very small momentum transfer $\mathbf{q}$. However, such a "brute-force" approach, besides adding significant computational overhead, in practice fails for a $\mathbf{q}$ small enough to address the Drude response in the far infrared, because of numerical instabilities due to the closeness in energy of the relevant initial and final states. To prevent such numerical instabilities we evaluate the difference of energies by an expansion of the dispersion to first order in $\mathbf{q}$. The explicit inclusion of the intraband transitions into the independent-particle response function allows, differently from plasma models, a full treatment of the CLF, plus the straightforward possibility to treat anisotropic systems. In particular we obtain an *ab initio* determination of the anisotropy in the static conductivity.

We apply this method to isotropic and magnetic bulk iron and to weakly anisotropic bulk magnesium. We compare the computed optical properties of bulk iron with the measurements obtained by ellipsometry,[13–17] reflectance,[18–20] optical absorption, and thermoreflectance.[21] Similarly, we compare the computed spectra of magnesium with experiments done on polycrystalline samples[15] and on single crystals,[22–24] where anisotropy is accessed.

This paper is organized as follows: in Sec. II we review the theoretical background and the method used to take the intraband transitions into full account. We proceed to discuss its application to iron in Sec. III and to magnesium in Sec. IV. We then discuss the results in Sec. V.

II. METHODS

In the equations, we adopt the standard system of atomic units, based on $m_e = \hbar = q_e^2/(4\pi\varepsilon_0) = 1$, so that, e.g., energies and angular frequencies are measured in Hartree (Ha), and lengths in Bohr radii (a_0). When displaying optical spectra, we will usually revert to more familiar electron volt energy units.

A. General background

The optical properties of solids are given by the long-wavelength limit of the macroscopic dielectric function,

which is obtained from the average of its inverse microscopic counterpart over a unit cell[25,26] as

$$\varepsilon_M(\mathbf{q},\omega) = \frac{1}{[\varepsilon^{-1}_{\mathbf{G},\mathbf{G}'}(\mathbf{q},\omega)]_{\mathbf{0},\mathbf{0}}}. \quad (1)$$

Here ε_M is the macroscopic dielectric function and $\varepsilon_{\mathbf{G},\mathbf{G}'}(\mathbf{q},\omega)$ is the microscopic one, which is a function of the radiation frequency ω and momentum $\mathbf{q}$, and a matrix indexed by the reciprocal-lattice vectors. The theoretical determination of the inverse microscopic dielectric function is usually based on the evaluation of the dynamical density-density response function χ, to which ε^{-1} is related by

$$\varepsilon^{-1}_{\mathbf{G},\mathbf{G}'}(\mathbf{q},\omega) = \delta_{\mathbf{G},\mathbf{G}'} + \mathrm{Tr}_\sigma[v_C(\mathbf{q}+\mathbf{G})\chi_{\sigma,\sigma'\mathbf{G},\mathbf{G}'}(\mathbf{q},\omega)], \quad (2)$$

where v_C is the Coulomb potential and σ,σ' are the spin variables. The time-dependent density-functional theory (TDDFT) in the linear-response regime[27,28] provides a standard method to compute χ. Within this approach, χ is the solution of the following Dyson-type equation

$$\chi_{\sigma,\sigma',\mathbf{G},\mathbf{G}'}(\mathbf{q},\omega) = \chi^{(0)}_{\sigma,\sigma',\mathbf{G},\mathbf{G}'}(\mathbf{q},\omega) + \sum_{\sigma_1,\sigma_2,\mathbf{G}_1,\mathbf{G}_2} \chi^{(0)}_{\sigma,\sigma_1,\mathbf{G},\mathbf{G}_1}(\mathbf{q},\omega)[v_c(\mathbf{q}+\mathbf{G}_1) + f_{xc\sigma_1,\sigma_2,\mathbf{G}_1,\mathbf{G}_2}(\mathbf{q},\omega)]\chi_{\sigma_2,\sigma',\mathbf{G}_2,\mathbf{G}'}(\mathbf{q},\omega). \quad (3)$$

The exchange and correlation kernel f_{xc} in Eq. (3) is defined as the functional derivative of the DFT exchange and correlation potential V_{xc} with respect to density.[29] As V_{xc} is known only approximately, also f_{xc} is. In the present work we assume the RPA, (i.e., $f_{xc}\equiv 0$). In this approximation, a direct relation of the dielectric response function to $\chi^{(0)}$ is well known[30]

$$\varepsilon^{\mathrm{RPA}}_{\mathbf{G},\mathbf{G}'}(\mathbf{q},\omega) = \delta_{\mathbf{G},\mathbf{G}'} - \mathrm{Tr}_\sigma[v_C(\mathbf{q}+\mathbf{G})\chi^{(0)}_{\sigma,\sigma'\mathbf{G},\mathbf{G}'}(\mathbf{q},\omega)]. \quad (4)$$

This assumption is reasonable for the study of optical spectroscopies, where the long-wavelength $\mathbf{q}\to\mathbf{0}$ limit applies: in this limit all standard more refined TDDFT kernel approximations are limited functions, which, at least for the $\mathbf{G}_1=\mathbf{0}$ terms are therefore tiny corrections[31] to the diverging Coulomb potential $v_c(\mathbf{q})=4\pi/|\mathbf{q}|^2$. We compute the independent-particle response function $\chi^{(0)}$ of Eq. (3), using the well-established expression[25,26]

$$\chi^{(0)}_{\sigma,\sigma',\mathbf{G},\mathbf{G}'}(\mathbf{q},\omega) = -\frac{1}{\Omega}\delta_{\sigma,\sigma'} \times \sum_{j,j'}\int_\Omega d^3k \frac{f[\epsilon_{j',\sigma}(\mathbf{k}+\mathbf{q})] - f[\epsilon_{j,\sigma}(\mathbf{k})]}{\omega^+ - [\epsilon_{j',\sigma}(\mathbf{k}+\mathbf{q}) - \epsilon_{j,\sigma}(\mathbf{k})]} \times \tilde{\rho}_{j,j',\sigma,\mathbf{G}}(\mathbf{k},\mathbf{q})\tilde{\rho}^*_{j,j',\sigma,\mathbf{G}'}(\mathbf{k},\mathbf{q}), \quad (5)$$

where $f(\epsilon)$ is the Fermi occupation distribution, $\tilde{\rho}_{j,j',\sigma,\mathbf{G}}(\mathbf{k},\mathbf{q})$ are the matrix elements $\langle \mathbf{k},j,\sigma|e^{-i(\mathbf{q}+\mathbf{G})\cdot\hat{\mathbf{r}}}|\mathbf{k}+\mathbf{q},j',\sigma\rangle$, and $\epsilon_{j,\sigma}(\mathbf{k})$ is the Kohn-Sham band energy corresponding to state $|\mathbf{k},j,\sigma\rangle$. The frequency ω^+ at the denominator includes a small imaginary part that accounts phenomenologically for the lifetime of the band states and helps the calculation to avoid the excitation poles. Equation (5) hence yields a causal response function in the complex ω space.

The long-wavelength limit $\mathbf{q}\to\mathbf{0}$ of Eq. (5), relevant for the optical properties, cannot be evaluated naively, due to the vanishing of specific factors in Eq. (5), namely: (i) for interband transitions ($j\neq j'$), the matrix element $\tilde{\rho}_{j,j',\sigma,\mathbf{G}}(\mathbf{k},\mathbf{q}\to\mathbf{0})$ vanishes for $\mathbf{G}=\mathbf{0}$ and (ii) for intraband terms ($j=j'$), it is the turn of the difference in occupancies to vanish. In both cases, the small-$\mathbf{q}$ asymptotics of $\chi^{(0)}$ provides the leading contribution in the multiplication of Eq. (4) by the diverging $v_c(\mathbf{q})=4\pi/|\mathbf{q}|^2$.

In the calculations for nonmetallic compounds, where only the first problem is relevant, the standard workaround to evaluate the correct limit of the matrix element[1,32] expands its operatorial part in this form

$$\langle \mathbf{k},j,\sigma|e^{-i\mathbf{q}\cdot\hat{\mathbf{r}}}|\mathbf{k}+\mathbf{q},j',\sigma\rangle = \delta_{j,j'} + \frac{\mathbf{q}\cdot\langle \mathbf{k},j,\sigma|i\nabla + i[V_{\mathrm{nl}},\mathbf{r}]|\mathbf{k},j',\sigma\rangle}{\epsilon_{j',\sigma}(\mathbf{k}) - \epsilon_{j,\sigma}(\mathbf{k})} + O(\mathbf{q})^2, \quad (6)$$

where the commutator $[V_{\mathrm{nl}},\mathbf{r}]$ is only needed when a nonlocal pseudopotential approach is used to account for the core electrons. This approach is valid also for interband contribution to the response function of metals.

The intraband ($j=j'$) transitions contribute to the response function $\chi^{(0)}$ of metallic bands, in a way which is difficult to evaluate numerically, because of the extremely small energy difference between $\epsilon_{j',\sigma}(\mathbf{k}+\mathbf{q})$ and $\epsilon_{j',\sigma}(\mathbf{k})$. This tiny energy difference produces a tiny difference in the occupancies in the numerator of Eq. (5), computed according to Fermi occupancy factors $f(\epsilon)$ for a small but finite fictitious electronic temperature T_{smear}. In the infrared region of frequencies, these tiny occupancy differences are the responsible for the actual value of the computed dielectric function and suffer greatly from the numerical noise in the determination of the band energies. In the present work we propose a numerically stable method to evaluate the intraband contribution of these transitions across the Fermi surface.

B. Intraband contribution

To compute the intraband contribution $\chi^{(0)\mathrm{intra}}$ to the independent-particle response function we expand in power of $\mathbf{q}$ both the matrix elements (as for the interband part) and the band dispersion $\epsilon_{j,\sigma}(\mathbf{k})$ in Eq. (5). We carry out this expansion around each $\mathbf{k}$ point of the mesh where we compute the Kohn-Sham eigenfunctions and eigenenergies. In order to preserve the time-reversal symmetry, it is convenient to use the expansion to estimate the band energies at the nearby points $\mathbf{k}\pm\mathbf{q}/2$ so that the contributions of points $\mathbf{k}$ and $-\mathbf{k}$ remain identical.

The power expansion of the intraband energy difference at the denominator of Eq. (5) takes hence the well-known form[33]

$$\Delta\epsilon_{j,\sigma}(\mathbf{k}) = \epsilon_{j,\sigma}\left(\mathbf{k}+\frac{1}{2}\mathbf{q}\right) - \epsilon_{j,\sigma}\left(\mathbf{k}-\frac{1}{2}\mathbf{q}\right) \simeq \mathbf{q}\cdot\nabla_{\mathbf{k}}\epsilon_{j,\sigma}(\mathbf{k}) + O(\mathbf{q})^3. \quad (7)$$

This expression allows us to evaluate also the difference of the occupancies at the numerator of Eq. (5). Rather than expanding the highly nonlinear Fermi function, we prefer to consider the small-$\mathbf{q}$ expansion of its argument and take the explicit difference

$$\Delta f_{j,\sigma}(\mathbf{k}) \simeq f\left[\epsilon_{j,\sigma}(\mathbf{k}) + \frac{\Delta\epsilon_{j,\sigma}(\mathbf{k})}{2}\right] - f\left[\epsilon_{j,\sigma}(\mathbf{k}) - \frac{\Delta\epsilon_{j,\sigma}(\mathbf{k})}{2}\right]. \quad (8)$$

The other ingredient in $\chi^{(0)\text{intra}}$, namely $\tilde{\rho}_{j,j,\sigma,\mathbf{G}}(\mathbf{k},\mathbf{q})$, has a finite $\mathbf{q}\to\mathbf{0}$ limit, which means that we can evaluate it directly at $\mathbf{q}=\mathbf{0}$, without the need of expansion (6) needed for the interband case $j\neq j'$. By observing that $\tilde{\rho}_{j,j,\sigma,\mathbf{G}}(-k,\mathbf{q}) = \tilde{\rho}_{j,j,\sigma,\mathbf{G}}(\mathbf{k},\mathbf{q})$, and putting everything together, the intraband contribution to the independent-electron polarizability takes the form

$$\chi^{(0)\text{intra}}_{\mathbf{G},\mathbf{G}'}(\mathbf{q},\omega) = -\frac{1}{2\Omega}\sum_j\sum_\sigma\int_\Omega d^3k\,\Delta f_{j,\sigma}(\mathbf{k})\left[\frac{1}{\omega^+ - \Delta\epsilon_{j,\sigma}(\mathbf{k})} - \frac{1}{\omega^+ + \Delta\epsilon_{j,\sigma}(\mathbf{k})}\right]\tilde{\rho}_{j,j,\sigma,\mathbf{G}}(\mathbf{k},\mathbf{0})\tilde{\rho}^*_{j,j,\sigma,\mathbf{G}'}(\mathbf{k},\mathbf{0}). \quad (9)$$

The summation in the square brackets implements the time-reversal symmetry even when the $\mathbf{k}$-point mesh does not.

When Eq. (9) is applied to the one band of the homogeneous electron gas, it produces the Lindhard function.[34] It is known[35,36] that the assumption of a constant imaginary part of the frequency ω^+ does not describe correctly the Drude behavior[37] of the imaginary part of the dielectric function ε_2 in the $\omega\to 0$ limit. In detail, $\varepsilon_2\propto\omega^{-3}$ (rather than the correct $\varepsilon_2\propto\omega^{-1}$) fails to reproduce the physical limit of a constant static conductivity but rather yields an unphysical diverging (as $\sim\omega^{-2}$) conductivity. This difficulty is not restricted to the homogeneous electron gas, but is a general property of Eq. (9), regardless of the underlying (metallic) band structure. In this paper we suggest a simple and rather natural solution of this problem, consisting in the calculation of $\chi^{(0)}$ along a path in the complex frequency plane not parallel to the real axis, i.e., we introduce a suitable frequency dependency of the imaginary part of ω^+. Explicitly, we take

$$\omega^+ = \sqrt{\omega(\omega+i\eta)} \quad (10)$$

with real ω. As sketched in Fig. 1, for sufficiently large $\omega \gg \eta$, we have an essentially constant imaginary part of $\omega^+ \simeq \omega + i\frac{\eta}{2}$, while for small $\omega < \eta$, we have

$$\omega^+ \simeq e^{i(\pi/4)}\sqrt{\eta\omega}\left(1 - \frac{i}{2}\frac{\omega}{\eta}\right) \quad (11)$$

with real and imaginary parts which tend to coincide in the small-frequency limit. For ε_2, this specific choice produces the expected smooth switching from the $\varepsilon_2\simeq\omega_p^2\eta/\omega^3$ (characteristic of the near-infrared region) to the small-frequency

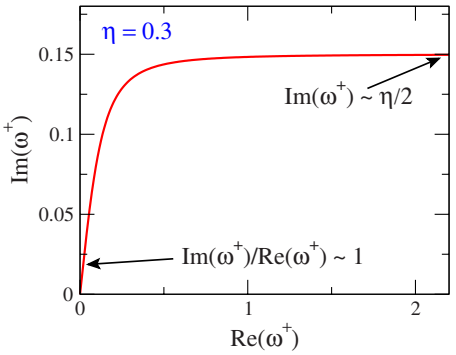

FIG. 1. (Color online) The path followed by the complex frequency ω^+, Eq. (10), to have Eq. (9) generate the correct Drude behavior of metallic solids.

Drude behavior $\varepsilon_2\simeq\omega_p^2/(\eta\omega)$, where ω_p is the plasma frequency. The parameter η accounts for all scattering processes that the electrons undergo and that attribute a finite lifetime to the Bloch states. Even though more refined and detailed methods to address the Drude behavior[36] are available, we suggest that the simple complex-plane path defined by Eq. (10) could be used effectively in all calculations of the response of metals.

In an actual numerical calculation of $\chi^{(0)\text{intra}}$, the crucial ingredient $\Delta\epsilon_{j,\sigma}(\mathbf{k})$ is evaluated according to Eq. (7) by means of the band-energy gradient, which is obtained in terms of the Bloch velocity matrix element[37]

$$\nabla_{\mathbf{k}}\epsilon_{j,\sigma}(\mathbf{k}) = \langle\mathbf{k},j,\sigma|\frac{d\mathbf{r}}{dt}|\mathbf{k},j,\sigma\rangle = \langle\mathbf{k},j,\sigma|i[H,\mathbf{r}]|\mathbf{k},j,\sigma\rangle = \langle\mathbf{k},j,\sigma|\mathbf{p}|\mathbf{k},j,\sigma\rangle + \langle\mathbf{k},j,\sigma|i[V_{\text{nl}},\mathbf{r}]|\mathbf{k},j,\sigma\rangle. \quad (12)$$

Similar to the standard expansion (6) of the matrix elements needed for interband terms, also Eq. (12) contains a nonlocal contribution whenever pseudopotentials are used.

C. Computation details

We start from the electronic ground states of Fe and Mg determined within the DFT in the local spin density approximation (LSDA) in the Perdew-Wang parameterization,[38] and using the respective experimental structures.[39] We carry out the calculations using the *ab initio* plane-wave package ABINIT,[40–42] and norm-conserving Troullier-Martins[43] pseudopotentials. With a cut-off energy $E_{\text{cut}}=30$ Ha for Fe and 15 Ha for Mg we obtain bands energies converged within 2 meV up to approximately 90 eV above the Fermi level.

For the ground-state calculations, we find that a shifted $16\times16\times16$ Monkorst-Pack $\mathbf{k}$-points mesh, represented by 140 points in the irreducible Brillouin zone (BZ) of iron and 270 of magnesium, provides good convergence with an occupancy smearing temperature $T_{\text{smear}}=0.007$ Ha for Fe and 0.005 Ha for Mg. We take the resulting Kohn-Sham wave functions and energies as the staring point for the linear-

response calculations, which we carry out according to the formulas described in Sec. II, which we implement in an in-house adaptation of the DP code.[44] For the TDDFT calculations we verify that a random sampling of the BZ converges faster than a uniform mesh.[45] In addition, a random sampling also makes it simpler to enlarge the **k**-point sampling systematically, if needed. A mesh of 40 000 random **k** points is generally sufficient, in association with a Fermi-function smearing of the electronic occupancies $f(\epsilon)$ based on a smearing temperature of $T_{\text{smear}}=1\times10^{-5}$ Ha $\simeq 0.27$ meV $\simeq 3.2$ K. CLF effects are taken into account according to Eq. (2) by inverting the ε matrix on a basis of 55 **G** vectors for iron and 43 **G** vectors for magnesium.

For cubic, thus isotropic, iron it is sufficient to evaluate the response functions at one small (but necessarily finite) transferred momentum that we arbitrarily set to $\mathbf{q}=(5.80,4.64,3.48)\times10^{-6}a_0^{-1}$. Indeed, we have verified that for a momentum of the same size but pointing in a different direction the resulting spectra are the same within the uncertainty related to the unsymmetrized **k**-point mesh. To evaluate the anisotropic response of magnesium we perform calculations for two polarization vectors: one in the hexagonal plane $[\mathbf{q}=(1.03,-0.60,0)\times10^{-7}a_0^{-1}]$ and one in the perpendicular direction $[\mathbf{q}=(0,0,0.63)\times10^{-7}a_0^{-1}]$. Of course, as we verified, the response function is the same for **q** within the entire *xy* plane. It is necessary to select **q** vectors of such a tiny length to avoid finite-**q** artifacts in the small-ω behavior of the response function.

While all parameters discussed above are not especially critical, and allow us to obtain stable and well-converged spectra through the whole frequency range investigated in the present work, a much more delicate role is played by the small imaginary part η of Eq. (10). η mimics the finite quasiparticle lifetime, mainly due to electrons scattering against phonons and/or crystal defects.[8] A microscopic fully *ab initio* approach to the lifetime contribution $\eta_{j'j,\sigma}(\mathbf{k}+\mathbf{q},\mathbf{k})$ of each pair of states in Eq. (5), would, in principle, require the evaluation of the electron-phonon and electron-defect coupling of each individual band state, a cumbersome procedure indeed. In the present work we assume phenomenological estimations of η based on the available experimental data. We shall content ourselves with allowing for different values of η for the intraband and interband contributions to $\chi^{(0)}$. For Fe, we adjust the *intra*band η to the infrared ellipsometry data of Refs. 15 and 16 (from 0.018 to 0.049 eV), obtaining $\eta=4.60$ meV. For Mg, the available data[15] in the range 0.25–0.35 eV are compatible with $\eta=140$ meV.[46] For both metals, we broaden the *inter*band contributions to the spectrum with a width $\eta=50$ meV that allows the spectral features to show in a way quite comparable to experiment.

III. IRON

A. Electronic structure

Figure 2 displays the computed spin-resolved band structure and the corresponding density of states (DOS). The converged DOS represented in Fig. 2 is obtained with a random sampling of 5000 **k** points in the whole BZ. At the Fermi level, the total DOS is $N_{E_F}=0.970$ states/eV/atom, significantly larger than the experimental value $N_{E_F}=0.503$ states/eV/atom.[47] This discrepancy was already discussed in previous work[48] and attributed to a mass enhancement due to interactions of electrons with phonons and magnons.

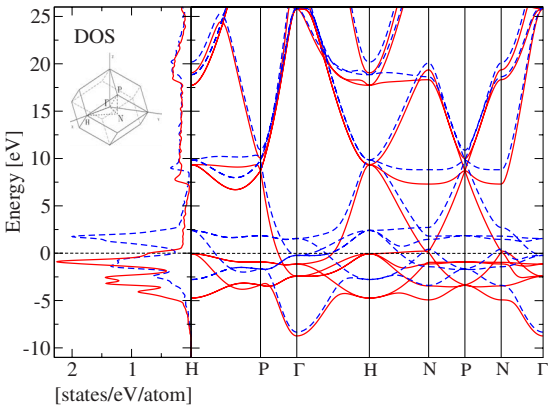

FIG. 2. (Color online) The spin-resolved DOS (left) and band structure of BCC iron computed along the standard high symmetry directions of the BZ, as depicted inside the BZ of a bcc crystal drawn in the inset. Majority electrons: solid lines; minority: dashed lines. The energy reference is taken at the Fermi level.

We compare our band structure with previous calculations[49–58] and with experimental data.[59,60] We verify that, even though LSDA and generalized gradient approximation would yield significant differences, in particular, in equilibrium structure,[61] the electronic properties calculated for the experimental lattice structure[62] within either approximations are similar, making LSDA satisfactory for our purposes. In particular, the DFT-LSDA calculations yield a magnetization of 2.20 μ_B per cell, very similar to the experimental magnetization of 2.22 μ_B.[60]

B. Excited-state properties

Figure 3 reports the computed dielectric function, and compares it to the one obtained by including intraband and interband contributions separately in $\chi^{(0)}$. Even though, due to CLF, the total dielectric function is not, strictly speaking, the sum of intraband and interband contributions, it is evident that intraband response dominates at low frequency $\omega<0.5$ eV, while interband takes over for optical frequencies. Note in particular that the infrared region (inset) displays the appropriate power laws, with the correct overall scale due to the value of η being fitted precisely to the near-infrared part of the experimental spectrum. Note the expected power-law crossover from $\varepsilon_2\simeq\omega_p^2/(\eta\omega)$ to $\varepsilon_2\simeq\omega_p^2\eta/\omega^3$ occurring near $\omega\simeq\eta$, reflecting the standard Drude behavior.[63]

Figure 3 compares the computed dielectric function to experimental data obtained by ellipsometry[15] and reflectance measurements.[19] The visible-UV region shows overall agreement of the few discernible experimental features. The features of the interband spectral are more evident in the optical conductivity

$$\sigma(\omega)=-i\frac{\omega}{4\pi}[\varepsilon(\omega)-1] \tag{13}$$

as reported in Fig. 4. The RPA spectrum displays prominent spectral features at 2.8, 5.2, 6.5, and 10.5 eV. In the 1–8 eV

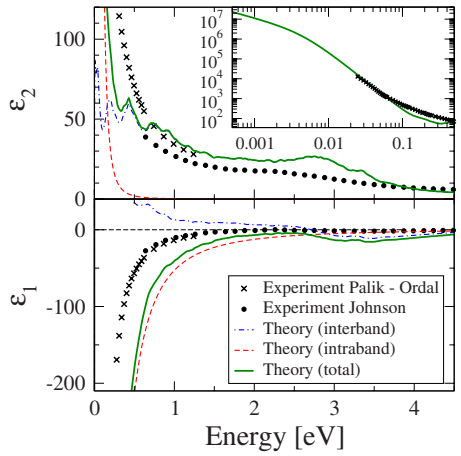

FIG. 3. (Color online) Imaginary (top) and real (bottom) parts of the computed dielectric function (solid) of iron, resolved in its interband (dot-dashed line) and intraband (dashed line) contributions. Experimental data from Ref. 15 (crosses) and 19 (dots) are reproduced for comparison. Inset: the infrared region in a log-log scale, displaying the $\propto\omega^{-1}$ and $\propto\omega^{-3}$ power-law behaviors of ε_2 in the far- and near-infrared regions.

range, computed features correspond to experimental ones appearing as a broad peak near 2.7 eV and minor features around 6 eV. Above 8 eV, the experimental data display a flat region with a weakly raising trend near 12 eV. The computed absolute value of σ and the general spectral shape are hence in fair agreement with the measured ones, especially below 8 eV. Discrepancies in the 8–12 eV features might be due to lifetime and correlation effects not accounted for in the present simple model,[10] and which might be captured by a more refined theoretical approach, such as GW (Refs. 65 and 66) or Bethe-Salpeter calculation.[67] A detailed analysis indicates that the structures around 2.8 and 6.5 eV are mainly due to the minority spin while the majority spin dominates the intraband contribution and the region above 8 eV.

The inset of Fig. 4 zooms into the intraband region, and shows, in particular, that the computed static conductivity

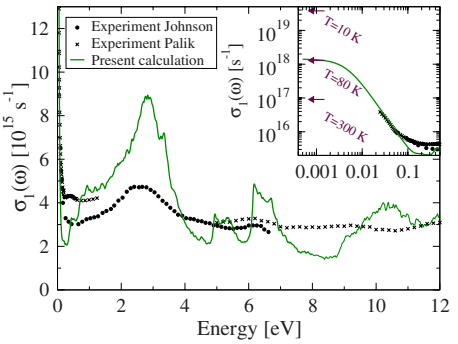

FIG. 4. (Color online) Comparison between optical conductivity measurements (Refs. 15 and 19) and the present calculation (RPA with the inclusion of CLF and intraband transitions). Inset: a log-log blowup of the low-energy region with the experimental static conductivity values at three temperatures (Ref. 64). For conductivity we use traditional inverse-second units but regular SI units $(\Omega\ \mathrm{m})^{-1}$ are retrieved immediately by multiplication by $4\pi\varepsilon_0 = 1.11\times10^{-10}$ s/(Ωm).

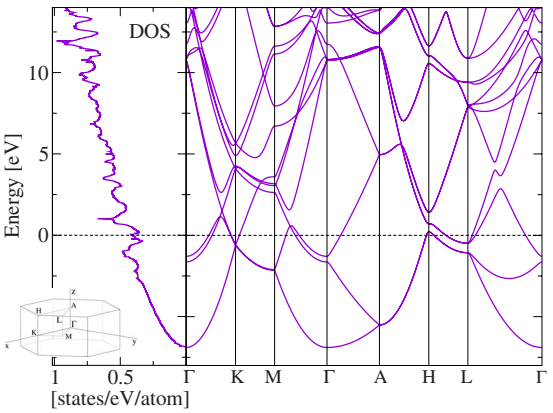

FIG. 5. (Color online) The DOS (left) and band structure of hcp magnesium computed along the path in the BZ, depicted in the inset. The energy reference is taken at the Fermi level.

$\sigma(0)=1.4\times10^{18}$ s^{-1}, equivalent to 1.55×10^{8} $(\Omega\ \mathrm{m})^{-1}$, falls in the range of measured low-temperature resistivities.[64] It is interesting to note that the considered lifetime $\tau=\hbar/\eta = 1.43\times10^{-13}$ s of the band states is substantially larger than the estimate that one would obtain from a free-electron model[37] $\tau_{\mathrm{fem}}=m_e\sigma(0)/(nq_e^2)=3.25\times10^{-14}$ s with the appropriate number density n, and the same static conductivity $\sigma(0)$.

IV. MAGNESIUM

A. Electronic structure

The starting point of the analysis of Mg is the calculation of its electronic structure, which we carry out for its experimental crystal structure.[68] The resulting band structure and the corresponding DOS (computed on a $16\times16\times16$ Monkorst-Pack mesh using the tetrahedron method), reported in Fig. 5, confirms that indeed Mg is a free-electron-like metal, as was already assessed by previous investigations.[69–71] Only weak asymmetries in the electron-gas response are therefore to be expected due to its hexagonal crystal structure.

B. Excited-state properties

The response function, computed for light polarized perpendicular and parallel to the hexagonal crystal c axis, is reported in Fig. 6. The calculations predict a significant anisotropy in the spectral region near 0.7 eV, mainly associated to interband transitions. In particular, near 0.7 eV the computed spectra predict a stronger absorption in the basal plane than along the c axis, in accord with single-crystal experimental evidence.[22–24]

The anisotropy in the Drude region is more evident in the optical conductivity as reported in Fig. 7. In this spectral region the anisotropy is opposite to the one of the 0.7 eV peak, namely, σ is larger for c-axis polarization than in the basal plane, but the difference is rather modest, of the order 30%. To resolve such a weak anisotropy the use of an explicit **k**-point mesh symmetrization was crucial.

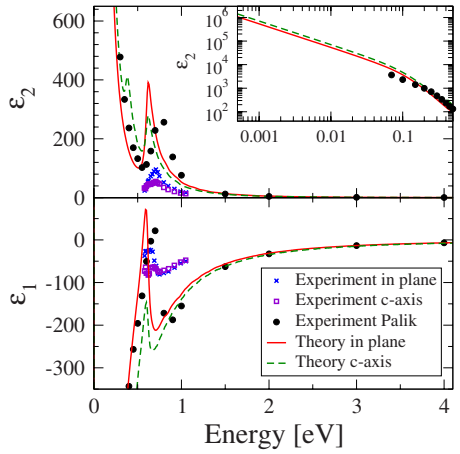

FIG. 6. (Color online) Imaginary (top) and real (bottom) parts of the computed dielectric function of magnesium in the basal plane (solid) and along the c axis (dashed). Experimental data from Ref. 15 (dots) and 22 (crosses and squares) are reproduced for comparison. Inset: the infrared region in a log-log scale, displaying the $\propto\omega^{-1}$ and $\propto\omega^{-3}$ power-law behaviors of ε_2 in the far- and near-infrared regions.

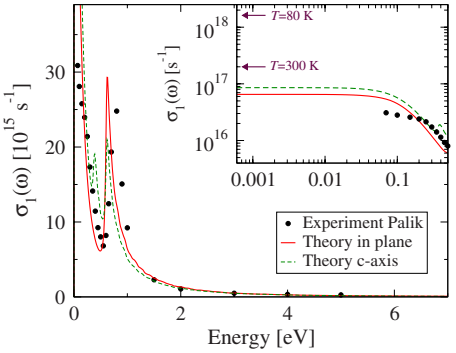

FIG. 7. (Color online) Computed optical conductivity in the basal plane (solid) and along the c axis (dashed), compared to measurements on polycrystalline magnesium samples (Ref. 15). Inset: a log-log blowup of the infrared region with the experimental static conductivity at two temperatures (Ref. 64). Units are like in Fig. 4.

The inset of Fig. 7 zooms into the intraband region, and shows, in particular, that the computed static conductivity $\sigma(0)=6.5\cdot10^{16}$ s^{-1} (in plane) and $\sigma(0)=8.7\times10^{16}$ s^{-1} (c axis), is slightly smaller than the measured room temperature resistivity of magnesium.[64] This is probably due to a overestimation of η as derived from the data of Ref. 15. The considered lifetime $\tau=\hbar/\eta=4.7\times10^{-15}$ s of the band states is in substantial agreement with the estimate that one would obtain from a free-electron model $\tau_{\rm fem}=m_e\sigma(0)/(nq_e^2)=3.3\times10^{-15}$ s, with the appropriate number density n and a direction averaged static conductivity $\sigma(0)$. The agreement of the simple free-electron formula here is much better than for iron, as is to be expected of a simple metal such as magnesium.

V. DISCUSSION

In this work we introduce a simple method, based on the linearization of the band dispersion, to deal with the *ab initio* calculation of the intraband contributions to the optical spectra of metals. Calculations within a simple RPA show significant accord with the experimentally observed spectral features, and, in particular, the infrared behavior is captured quantitatively. The introduction of a scattering rate for the electrons at the Fermi level as the one phenomenological parameter needed to describe the finite lifetime of the band states and the use of an appropriate path in the complex-ω plane allow us to compute seamlessly the conductivity from the optical region down to the infrared range and to its static limit. In noncubic metals such as magnesium, the determination of the anisotropic optical conductivity is straightforward, without the need to resort to artificial parametrization involving, for example, multiple plasmon energies.[72]

As a technical, but significant, point, within the adopted plane-wave pseudopotential scheme, we observe that it is essential to include the nonlocal part of the pseudopotential in the calculation of both interband and intraband contributions to the spectra, as it was noted for the interband transitions of copper.[10] In particular, for iron we verified that the omission of the nonlocal part of the pseudopotential produces a substantial distortion of the spectrum, especially in the 0.5–2 eV range, where ε_1 even acquires the wrong sign. Note however that the proposed approach is not restricted to this basis scheme, but can be used, for example, in an all-electron calculation.

ACKNOWLEDGMENTS

We acknowledge support by the Italian MIUR through PRIN-20079XA4HW, by the European Union through the ETSF-I3 project (Contract No. 211956) and by CINECA-Italy through a Supercomputing grant. L.C. thanks the Università Italo-Francese for the financial support through the "Borsa Vinci 2006." We thank R. Del Sole, A. Marini, E. Mulazzi, L. Reining, and F. Sottile for useful discussions.

*marco.cazzaniga@unimi.it
†lucia.caramella@unimi.it

[1] M. S. Hybertsen and S. G. Louie, Phys. Rev. B **35**, 5585 (1987).
[2] G. Onida, L. Reining, and A. Rubio, Rev. Mod. Phys. **74**, 601 (2002).
[3] L. Reining, V. Olevano, A. Rubio, and G. Onida, Phys. Rev. Lett. **88**, 066404 (2002).
[4] W. G. Schmidt, S. Glutsch, P. H. Hahn, and F. Bechstedt, Phys. Rev. B **67**, 085307 (2003).
[5] H.-V. Nguyen and S. de Gironcoli, Phys. Rev. B **79**, 205114 (2009).
[6] H. F. Wilson, D. Lu, F. Gygi, and G. Galli, Phys. Rev. B **79**, 245106 (2009).
[7] B. Walker, A. M. Saitta, R. Gebauer, and S. Baroni, Phys. Rev. Lett. **96**, 113001 (2006).
[8] K.-H. Lee and K. J. Chang, Phys. Rev. B **49**, 2362 (1994).
[9] E. G. Maksimov, I. I. Mazin, S. N. Rashkeev, and Y. A. Uspensky, J. Phys. F: Met. Phys. **18**, 833 (1988).

[10] A. Marini, G. Onida, and R. Del Sole, Phys. Rev. B **64**, 195125 (2001).
[11] C. Ambrosch-Draxl and J. O. Sofo, Comput. Phys. Commun. **175**, 1 (2006).
[12] J. A. Berger, P. Romaniello, R. van Leeuwen, and P. L. de Boeij, Phys. Rev. B **74**, 245117 (2006).
[13] H. T. Yolken and J. Kruger, J. Opt. Soc. Am. **55**, 842 (1965).
[14] G. A. Bolotin, M. M. Kirillova, and V. M. Mayevskiy, Phys. Met. Metallogr. **27**, 31 (1969).
[15] E. D. Palik, *Handbook of Optical Constants of Solids* (Academic Press, San Diego, 1998).
[16] M. A. Ordal, Appl. Opt. **22**, 1099 (1983).
[17] A. S. Siddiqui and D. M. Treherne, Infrared Phys. **17**, 33 (1977).
[18] A. J. Blodgett and W. E. Spicer, Phys. Rev. **158**, 514 (1967).
[19] P. B. Johnson and R. W. Christy, Phys. Rev. B **9**, 5056 (1974).
[20] T. J. Moravec, J. C. Rife, and R. N. Dexter, Phys. Rev. B **13**, 3297 (1976).
[21] J. H. Weaver, E. Colavita, D. W. Lynch, and R. Rosei, Phys. Rev. B **19**, 3850 (1979).
[22] D. Jones and A. H. Lettington, Proc. Phys. Soc. **92**, 948 (1967).
[23] A. P. Lenham and D. M. Treherne, J. Opt. Soc. Am. **56**, 752 (1966).
[24] R. H. W. Graves and A. P. Lenham, J. Opt. Soc. Am. **58**, 126 (1968).
[25] S. L. Adler, Phys. Rev. **126**, 413 (1962).
[26] N. Wiser, Phys. Rev. **129**, 62 (1963).
[27] M. A. L. Marques and E. K. U. Gross, Annu. Rev. Phys. Chem. **55**, 427 (2004).
[28] S. Botti, A. Schindlmayr, R. Del Sole, and L. Reining, Rep. Prog. Phys. **70**, 357 (2007).
[29] M. A. L. Marques, C. A. Ullrich, F. Ngueira, A. Rubio, K. Burke, and E. K. U. Gross, *Time-Dependent Density Functional Theory*, Lecture Notes in Physics (Springer, Heidelberg, 2006).
[30] G. F. Giuliani and G. Vignale, *Quantum Theory of the Electron Liquid* (Cambridge University Press, Cambridge, England, 2005).
[31] K. Tatarczyk, A. Schindlmayr, and M. Scheffler, Phys. Rev. B **63**, 235106 (2001).
[32] G. Grosso and G. Pastori Paravicini, *Solid State Physics* (Academic Press, San Diego, 2003).
[33] J. M. Ziman, *Principles of the Theory of Solids* (Cambridge University Press, Cambridge, England, 1964).
[34] A. L. Fetter and J. D. Walecka, *Quantum Theory of Many Particle Systems* (Dover, New York, 2003).
[35] P. Garik and N. W. Ashcroft, Phys. Rev. B **21**, 391 (1980).
[36] G. S. Atwal and N. W. Ashcroft, Phys. Rev. B **65**, 115109 (2002).
[37] N. W. Ashcroft and N. D. Mermin, *Solid State Physics* (Harcourt College, Orlando, 1976).
[38] J. P. Perdew and Y. Wang, Phys. Rev. B **45**, 13244 (1992).
[39] The lattice parameter of iron is assumed $a=5.42a_0$ (Ref. 62). The hcp structure of magnesium has $a=6.06a_0$ and $c=9.85a_0$ (Ref. 68).
[40] X. Gonze, G.-M. Rignanese, M. Verstraete, J.-M. Beuken, Y. Pouillon, R. Caracas, F. Jollet, M. Torrent, G. Zerah, M. Mikami, Ph. Ghosez, M. Veithen, V. Olevano, L. Reining, R. Godby, G. Onida, D. Hamann, and D. C. Allan, Z. Kristallogr. **220**, 558 (2005).
[41] X. Gonze, B. Amadon, P.-M. Anglade, J.-M. Beuken, F. Bottin, P. Boulanger, F. Bruneval, D. Caliste, R. Caracas, M. Côté, T. Deutsch, L. Genovese, Ph. Ghosez, M. Giantomassi, S. Goedecker, D. R. Hamann, P. Hermet, F. Jollet, G. Jomard, S. Leroux, M. Mancini, S. Mazevet, M. J. T. Oliveira, G. Onida, Y. Pouillon, T. Rangel, G.-M. Rignanese, D. Sangalli, R. Shaltaf, M. Torrent, M. J. Verstraete, G. Zerah, and J. W. Zwanziger, Comput. Phys. Commun. **180**, 2582 (2009).
[42] The ABINIT code is a common project of the Université Catholique de Louvain, Corning Incorporated, and other contributors, http://www.abinit.org
[43] N. Troullier and J. L. Martins, Phys. Rev. B **43**, 1993 (1991).
[44] http://www.dp-code.org
[45] S. Albrecht, L. Reining, G. Onida, V. Olevano, and R. Del Sole, Phys. Rev. Lett. **83**, 3971 (1999).
[46] Other experiments (Ref. 23) find a narrower Drude peak, compatible with a smaller value of $\eta \approx 50$ meV.
[47] M. Dixon, F. E. Hoare, T. M. Holden, and D. E. Moody, Proc. R. Soc. London, Ser. A **285**, 561 (1965).
[48] T. Nautiyal and S. Auluck, Phys. Rev. B **34**, 2299 (1986).
[49] J. Callaway, Phys. Rev. **99**, 500 (1955).
[50] J. H. Wood, Phys. Rev. **126**, 517 (1962).
[51] L. F. Mattheiss, Phys. Rev. **134**, A970 (1964).
[52] R. A. Tawil, Phys. Rev. B **7**, 4242 (1973).
[53] M. Singh, C. S. Wang, and J. Callaway, Phys. Rev. B **11**, 287 (1975).
[54] H. Yamagami, J. Phys. Soc. Jpn. **67**, 3176 (1998).
[55] J. Callaway and C. S. Wang, Phys. Rev. B **16**, 2095 (1977).
[56] H. S. Greenside and M. A. Schlüter, Phys. Rev. B **27**, 3111 (1983).
[57] E. G. Moroni, G. Kresse, J. Hafner, and J. Furthmüller, Phys. Rev. B **56**, 15629 (1997).
[58] M. Cococcioni and S. de Gironcoli, Phys. Rev. B **71**, 035105 (2005).
[59] A. M. Turner, A. W. Donoho, and J. L. Erskine, Phys. Rev. B **29**, 2986 (1984).
[60] J. F. van Acker, Z. M. Stadnik, J. C. Fuggle, H. J. W. M. Hoekstra, K. H. J. Buschow, and G. Stroink, Phys. Rev. B **37**, 6827 (1988).
[61] D. J. Singh, W. E. Pickett, and H. Krakauer, Phys. Rev. B **43**, 11628 (1991).
[62] R. Kohlhaas, P. Donner, and N. Schmitz-Pranghe, Z. Angew. Phys. **23**, 245 (1967).
[63] Our calculations are consistent with an intraband plasma frequency of iron $\omega_p=7.08$ eV. For Mg we find a value of $\omega_p=8.5$ eV in the plane and of $\omega_p=9.8$ eV along the c axis.
[64] R. C. Weast and M. J. Astle, *CRC Handbook of Chemistry and Physics*, 63rd edition (CRC Press, Boca Raton, Florida, 1982).
[65] A. Marini, G. Onida, and R. Del Sole, Phys. Rev. Lett. **88**, 016403 (2001).
[66] M. Cazzaniga, N. Manini, L. G. Molinari, and G. Onida, Phys. Rev. B **77**, 035117 (2008).
[67] A. Marini and R. Del Sole, Phys. Rev. Lett. **91**, 176402 (2003).
[68] G. B. Walker and M. Marezio, Acta Metall. **7**, 769 (1959).
[69] I. Baraille, C. Pouchan, M. Causà, and F. Marinelli, J. Phys.: Condens. Matter **10**, 10969 (1998).
[70] P. Blaha, K. Schwarz, and P. H. Dederichs, Phys. Rev. B **38**, 9368 (1988).
[71] E. Wachowicz and A. Kiejna, J. Phys.: Condens. Matter **13**, 10767 (2001).
[72] A. H. Reshak and S. Auluck, Phys. Rev. B **68**, 245113 (2003).